OUKA
The University of Osaka
Institutional Knowledge Archive

Title	High Temperature Creep of a 20Cr-25Ni Stainless Steel with Carbide Precipitation : Quantitative Analysis of the Precipitates and Theoretical Study of the Steady State Creep(Materials, Metallurgy & Weldability)
Author(s)	Takahashi, Makoto; Inoue, Katsunori; Yamane, Toshimi et al.
Citation	Transactions of JWRI. 1992, 21(2), p. 223-232
Version Type	VoR
URL	https://doi.org/10.18910/7118
rights	
Note	

The University of Osaka Institutional Knowledge Archive : OUKA

https://ir.library.osaka-u.ac.jp/

The University of Osaka

High Temperature Creep of a 20Cr-25Ni Stainless Steel with Carbide Precipitation†

— Quantitative Analysis of the Precipitates and Theoretical Study of the Steady State Creep —

Yasuo TAKAHASHI*, Katsunori INOUE, Toshimi YAMANE*** and Koichi NAKAGAWA******

Abstract

The variations in the steady state creep behaviour with temperatures (1053～1213K) for 20Cr-25Ni austenitic stainless steel are reported. Specimens in the solution treated condition (30min. at 1473K) were crept in air over the applied stress range 13.4～44.1MPa.

The apparent activation energy in the lower temperature region is approximately equal to the activation energy for self-diffusion of Fe, but that in the higher temperature region is stress sensitive, increasing with increasing stress. It is indicated that the creep deformation mechanism under the lower stress level is independent of the test temperatures, being the diffusion controlled dislocation creep, and that in the higher stress condition the rate controlling process changes from the diffusional recovery to the glide of mobile dislocations at the transition temperature, T_E. This is supported by analyzing the experimental results of the strain dip tests and characterizing the distribution of carbide precipitates.

KEY WORDS :(Austenitic Stainless Steel) (Creep) (Carbide) (Precipitate) (Diffusion)

1. Introduction

Many investigations of creep in austenitic stainless steels have been performed, most of them having been carried out in the temperature region 873 ～ 1073K[1-12]. There have not been a number of studies of the high temperature creep for 20Cr - 25Ni austenitic stainless steels in the temperature range from 1073 to 1213K[13]. It is, therefore, necessary to investigate the relationship between the steady state creep rate, $\dot{\varepsilon}_s$, and temperature in this range.

In general, $\dot{\varepsilon}_s$ can be described by the following equation[14]

$$\dot{\varepsilon}_s = A \sigma_a^n \exp(-Q_c / RT) \quad (1)$$

where n is the stress exponent, σ_a the applied stress, Q_c the activation energy, R the gas constant, T the absolute temperature, and A a constant. For pure metals, n is usually in the range 4～5, and Q_c is found to equal the activation energy for self-diffusion[15]. Stress exponents much higher than 4 ～ 5 were obtained for austenitic stainless steels[6,9,10,12] in using eq. (1). And also, the values of Q_c greater than that of self-diffusion have been obtained. The higher Q_c was explained by I.R. Mclauchlin[9] from the view of the pinning effect of small carbide particles,which acted as obstacles to dislocation glide and exerted the internal back stress, σ_i.

The steady state creep rate of 20Cr-25Ni austenitic stainless steels can therefore be more meaningfully represented by

$$\dot{\varepsilon}_s = A (\sigma_a - \sigma_i)^{n_e} \exp(-Q_c^* / RT) \quad (2)$$

where n_e is an effective stress exponent, independent of T and σ_a with a value of ～4, and Q_c^* is independent of σ_a.

In the recent years, J.P. Poirier reported the interpretation of strain dip tests[16], followed by M. Pahutovà et al[17]. In the light of their analyses, the present paper describes the creep deformation mechanisms for a 20Cr-25Ni austenitic stainless steel over the temperature range 1053～1213K, with the help of the strain dip tests and the quantitative analyses of carbide precipitates formed during creep.

2. Experimental Procedures

2.1 Specimen Preparation and Creep Tests

The chemical composition of the austenitic stainless steel used in the present study is given in Table 1. The rod specimens with the gauge length of 50mm and the diameter of 2.0mm were made of hot drawn wires, and annealed at 1473K for 30min., terminated by a water quench. The average grain diameter thus obtained was 100 μm.

† Received on Oct.31,1992

* Associate professor
** Professor
*** Professor, Fculty of Eng. Dept of Mater. Sci. and Eng.
**** Komatsu Seisakusho

Transactions of JWRI is published by Welding Research Institute, Osaka University, Ibaraki, Osaka 567, Japan

Table 1 Chemical composition

Cr	Ni	C	Mn	Si	P	S	Cu
19.24	25.43	0.12	1.82	0.51	0.09	0.10	1.81

Creep tests were carried out in air by using a load-creep machine, after heating for 1 hour at each test temperature. The strain rate was measured by a dial gauge to an accuracy of 0.01mm. The test temperature and stress range were mainly 1053～1213K and 13.4～44.1 MPa, respectively. The test temperature was maintained constant at within ± 0.5K during each test, and the gradient along the specimen was controlled to within 1K.

2.2 Structural Examination

Optical microstructure was observed on a longitudinal section of the specimen which had been cooled under load after the creep test. Optical micrographs were taken at a magnification of 600 times, when the mean size of precipitates was measured, and also at a magnification of 200 times when the precipitate distribution was examined.

The precipitate density in matrix was determined from the number of particles cut by a straight line on the photographs. This gave the number of particles per unit length, N_{LM}. The average precipitate (effective area) diameter, δ_M was measured from the particles cut along each line. According to Fullman[18] and Gates et al.[19], the number of matrix particles per unit volume was given by

$$N_{VM} = \frac{4N_{LM}}{\pi \delta_M^2} \quad (3)$$

The volume of matrix precipitate per unit volume was obtained by

$$V_{VM} = \frac{2}{3} N_{LM} \delta_M \quad (4)$$

In calculating the parameters of the precipitates dotted on grain boundaries, the parameters were estimated in accordance with the method proposed by Gates and Horton[19], although the volume of the elliptical particle was assumed to be $\frac{4}{3}\pi a^2 b$ in the present study, where a and b are the semi-major and semi-minor axies of the ellipse, respectively. The effective area diameter, δ_B was $2\sqrt{ab}$. The number of dotted-boundary particles per unit area of grain boundary, N_{AB}, was obtained from

$$N_{AB} = \frac{4N_{LB}}{\pi \delta_B} \sqrt{\frac{b}{a}} \quad (5)$$

where N_{LB} is the number of dotted-particles per unit length of the intersection of grain boundary with a longitudinal section of the specimen. The volume of the dotted-boundary precipitates per unit area of grain boundary (R.S.Gates et al gave $V_{ABD} = \frac{2}{3} N_{LB} \delta_B^2$ (b/a), by assuming that the volume of the elliptical particle was $\frac{4}{3}\pi ab^2$) was estimated by

$$N_{ABD} = \frac{2}{3} N_{LB} \delta_B^2 \quad (6)$$

On the other hand, the volume of the plate-like precipitate per unit area of grain boundary was expressed by

$$V_{ABP} = w \quad (7)$$

where w is the average thickness of the plate-like precipitate. In determining eqs. (5) and (6), it was assumed that the boundary precipitates increased so that they could enlarge a rather than b until they were distributed closely to each other on grain boundaries ($N_{ABD} = 1/2a$, $V_{ABD} = 4b/3 \simeq 2w/3$), and grew up to be the plate-like precipitate, as the temperature decreased.

When the dotted-precipitates and plate-like precipitates were observed on different grain boundaries of the same specimen, the idea of fraction was introduced, and then the volume of boundary precipitate per unit area of grain boundary was obtained from

$$V_{AB} = f_D V_{ABD} + f_P V_{ABP} \quad (8)$$

where f_D is the fraction of the grain boundaries on which the dotted-precipitates were distributed, and f_P ($= 1-f_D$) is the fraction of the grain boundaries at which the plate-like precipitate were observed. The volume of boundary precipitate per unit volume was described by

$$V_{VB} = V_{AB} \cdot S_V \quad (9)$$

where S_V is the boundary area per unit volume and is expressed by

$$S_V = 2/d \quad (10)$$

where d is the average intercept grain diameter[19].

These precipitates were mostly identified as $M_{23}C_6$ type carbides by the X ray diffraction of the residual powder obtained with the electrolytic extraction. In that stage, the characteristic X ray, CrK α, was used[9,20]. X ray powder pattern incidentally exhibited weak M_7C_3 peaks and very weak peaks which could not be determined.

Transmission electron microscopy examination was performed on electrolytically thinned specimens, using the Hitachi HU-11A electron microscope operated at an accelerating voltage of 100 kV.

2.3 Orowan Stress

The number of matrix perticles per unit area of the slip plane of mobile dislocations is obtained by

$$N_S = \frac{4}{\pi} \cdot \frac{N_{LM}}{\delta_M} \tag{11}$$

The average effective spacing, λ, between matrix particles in the slip plane is determined from

$$\lambda = N_S^{-1/2} - \delta_M \tag{12}$$

The stress necessary for the dislocation to bow out around matrix particles is represented by

$$\sigma_o = \overline{M}\,\tau_o \tag{13}$$

where $\overline{M}$ is the average Taylor factor, and $\tau_o = 0.84 \cdot \frac{\mu b}{\lambda}$, proposed by U.F. Kocks[21]. If Orowan stress is estimated with $\overline{M} = 2$[12],

$$\sigma_o = 1.68 \cdot \frac{\mu b}{\lambda} \tag{14}$$

$\overline{M}$ is, however, expected to be $\geqq 3$, if the fcc polycrystal is deformed continuously[22].

2.4 Measurement of Internal Back Stress, σ_i

The strain dip tests were carried out, as likely as Refs.(10) and (23), on specimens which reached the steady state creep stage with the constant creep rates. The strain rate was measured in an accuracy of 0.001 mm.

In the stress drop tests, the upper and lower critical stresses, σ_p and σ_n, were defined as follows; $\sigma_p = \sigma_a - \Delta\sigma_p$, and $\sigma_n = \sigma_a - \Delta\sigma_n$, where σ_a is the initial applied stress, $\Delta\sigma_p$ and $\Delta\sigma_n$ shown in Fig.1. The positive creep rate was measured immediately after a stress decrement, $\Delta\sigma < \Delta\sigma_p$, and the negative creep rate was measured immediately after $\Delta\sigma \geqq \Delta\sigma_n$. If a stress decrement, $\Delta\sigma$, was between $\Delta\sigma_p$ and $\Delta\sigma_n$, zero creep rate was measured.

When the difference between σ_p and σ_n was small, σ_i could be defined as an average of σ_p and σ_n, by assuming that σ_p and σ_n are idealistically equal to σ_i. Of course, $\sigma_i = \sigma_a$, if $\sigma_p \simeq \sigma_a$, according to Refs.16,24 and 25.

If σ_i is estimated and the variation of $\dot{\epsilon}_s$ is rearranged with the effective stress, σ_e, the true activation energy for creep can be obtained by

$$Q_c^* = -R \left[\frac{\partial \ln \dot{\epsilon}_s}{\partial 1/T}\right] \sigma_e \tag{15}$$

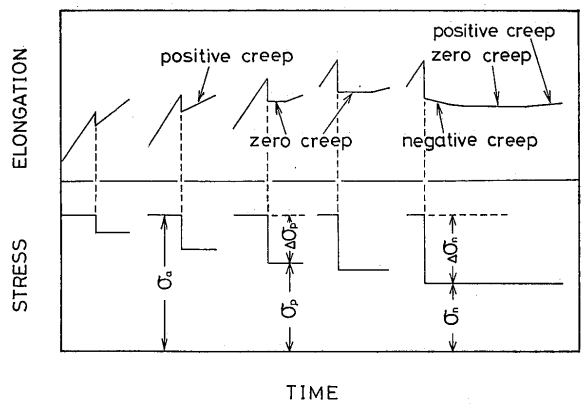

Fig.1 Transient strain response to the stress decrement, $\Delta\sigma$. This illustrate is one obtained from the data for σ_a = 34.7MPa, T = 1173K.

3. Experimental Results

3.1 Creep Curve

Fig.2 shows examples of the primary creep curves. One of them exhibits an incubation period where the creep rate is much less than the secondary creep rate. The creep curves at the stress levels lower than σ_a=24.7MPa have an incubation period in the temperature range 1053 ~1133K. The creep curves for σ_a = 44.1MPa, 1153K $\leqq$ T $\leqq$ 1213K become a straight line, in contrast with the normal creep curves which exhibit the transition creep stage. All of the primary creeps under the stress range of $\sigma_a \leqq$ 44.1MPa, are followed by the quasi-steady state creep.

3.2 Temperature Dependence of Steady State Creep Rate

The temperature dependence of the steady state creep rate, $\dot{\epsilon}_s$, for 13.4 $\leqq \sigma_a \leqq$44.1MPa is shown in Fig.3. These data can be approximated well by two straight lines. The transition temperature T_E[26] suggests a change in creep mechanisms. It appears that T_E is in the range of 1153 ~1173K, (Maybe, $T_E \simeq$ 1163K). At temperatures lower than T_E, the apparent activation energy, Q_c, for the creep under each applied stress is approximately equal to the activation energy, ΔH_{SD}, for self-diffusion of Fe

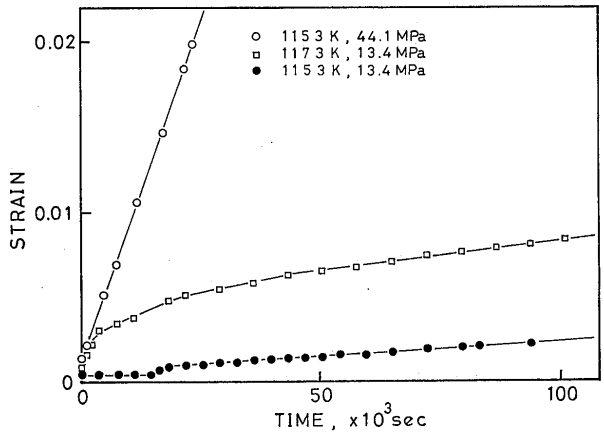

Fig.2 Examples of the primary creep curves

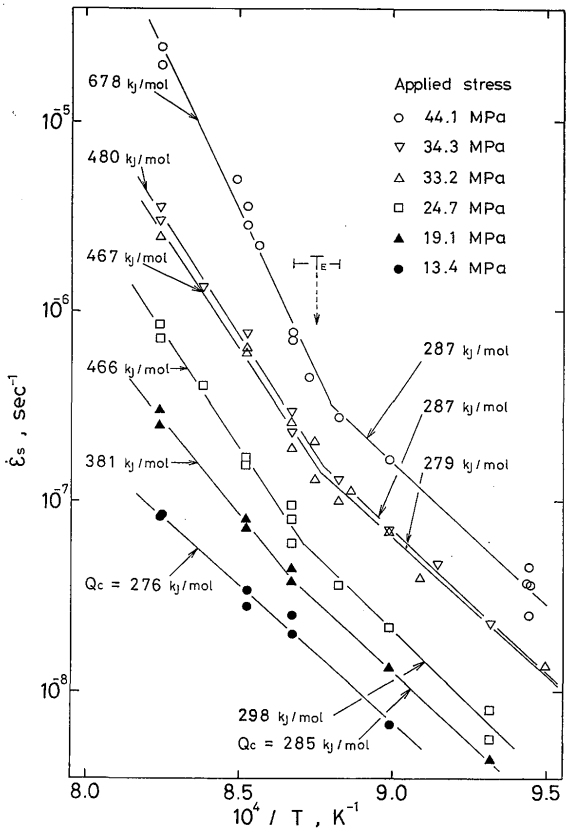

Fig.3 Temperature dependence of the steady state creep rate, $\dot{\varepsilon}_s$, at various applied stresses

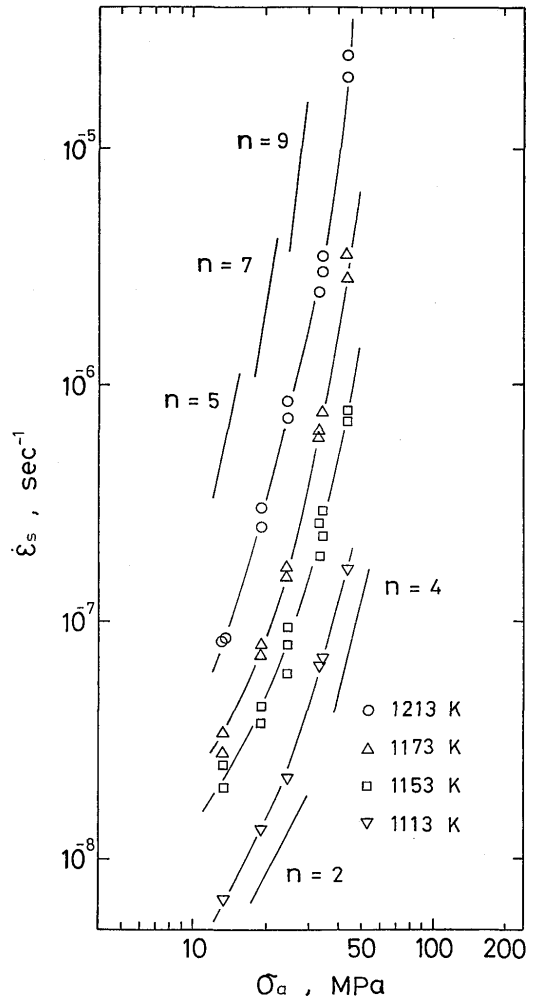

Fig.4 Stress dependence of the steady state creep rate, $\dot{\varepsilon}_s$, at various temperatures

(ΔH_{SD} =285kJ/mol)[15]. At temperatures above T_E, Q_c gradually increases as the applied stress increases. The experimental points for σ_a = 13.4 MPa in Fig.3 lie on the same straight line, and this line has no transition. These results are explained by the quantitative analyses of precipitates formed during the creep.

3.3 Stress Dependence of Steady State Creep Rate

The dependence of $\dot{\varepsilon}_s$ on σ_a is shown on a log-log plot in Fig.4, in order to be compared with the values of n in eq. (1). The slopes, n, of the curves increase as the applied stress increases. The stress dependencies at the higher temperatures are larger than those at the lower temperatures. This suggests a change in the creep deformation process with increasing stress and temperature.

3.4 Microstructures

The representative optical microstructures in the steady state creep region are shown in Fig. 5. Carbide precipitation occurs during creep in all the tests. The amount of precipitation on grain boundaries decreases with increasing test temperature. The morphology of boundary precipitates changes from the plate-like precipitate to the dotted-one at temperatures adjacent to T_E. The temperature dependences of N_{VM}, V_{VM}, V_{AB}, V_{VB}, and V_{total} (= V_{VM} + V_{VB}) are shown in Figs.6,7 and 8. All of these parameters decrease as the test temperature increases. No stress effects on these parameters were observed in the present study. This is due to the applied stress level much lower than that of Ref. (12).

In specimens tested at temperatures below T_E, dislocation tangles and pile-ups were observed at location adjacent to grain boundaries, as shown in Fig.9 (a), and the width of the fields of them increases with increasing σ_a, but there was no subgrains. On the other hand, such tangles were not observed in specimens tested at temperatures above T_E (Fig.9 (b)). Dislocation densities

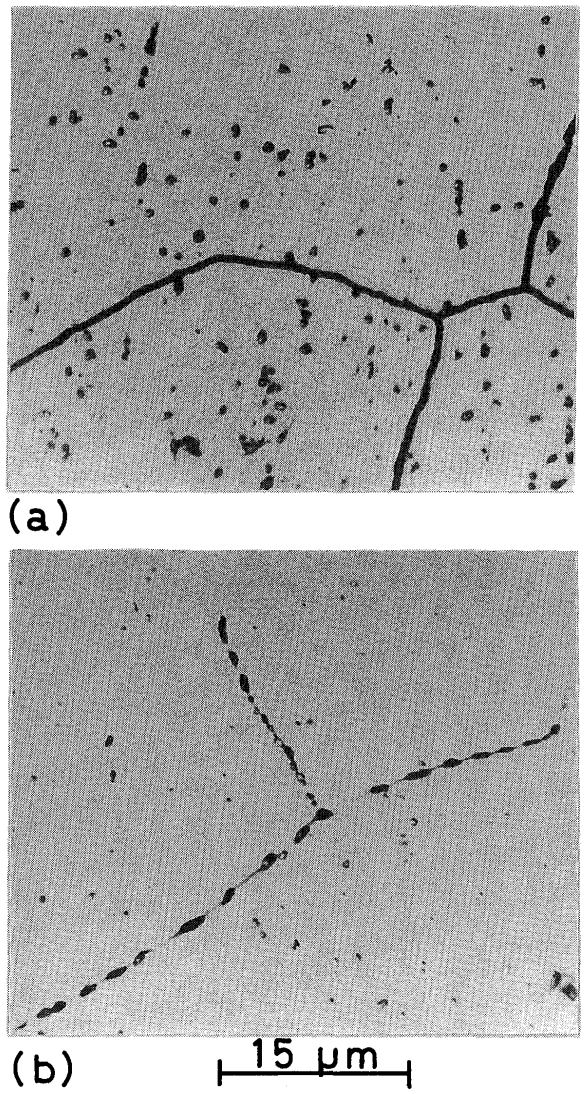

Fig.5 Optical microstructures in the steady state creep region ($\varepsilon \simeq 0.03$), (a)T = 1073K, σ_a = 24.7MPa, Plate-like precipitates in grain boundaries, (b) T = 1173K, σ_a = 24.7MPa, Dotted-precipitates in grain boundaries

in $T > T_E$ were much lower than those in $T < T_E$. This tendency becomes more obvious, as the applied stress increases.

3.5 Orowan Stress

The variations of λ and Orowan stress, σ_o with test temperature are shown in Fig.10. The values of σ_o are calculated from eq. (14). But, in fact, $\overline{M}$ is expected to be greater than 2 and rather close to 3, because the amount of grain-rotation will be small, even if it occurs during creep. At least, Fig .10 indicates that the Orowan stress at $T > T_E$ is much lower than that of $T < T_E$.

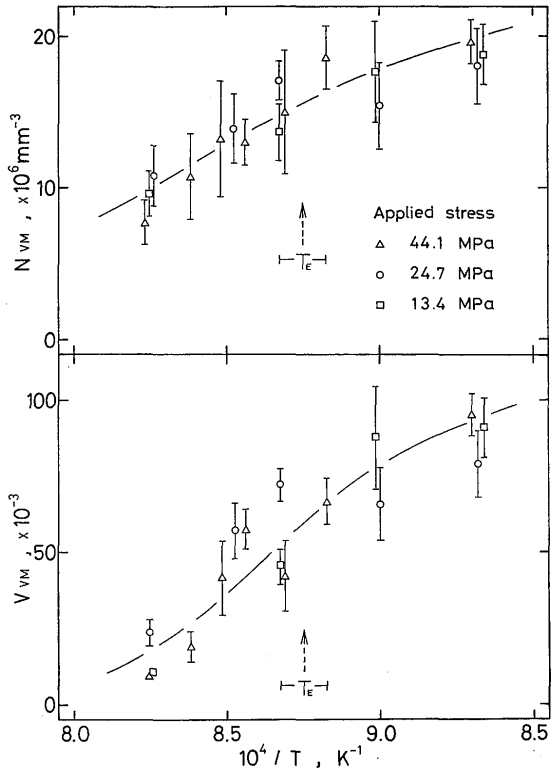

Fig.6 The variation of N_{VM} and V_{VM} with test temperature

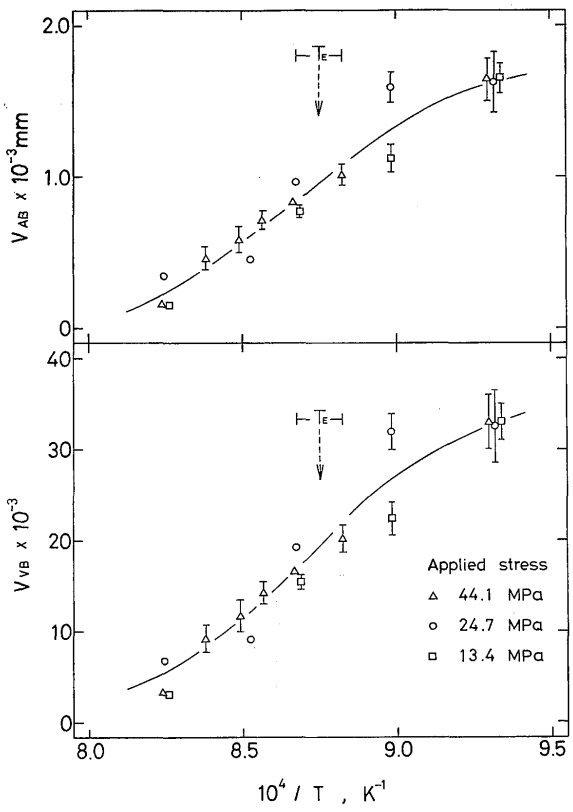

Fig.7 The variation of V_{AB} and V_{VB} with test temperature

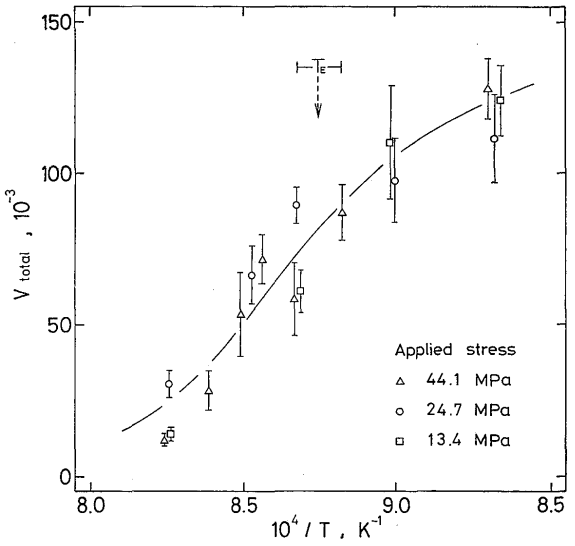

Fig.8 The variation of V_{total} with test temperature

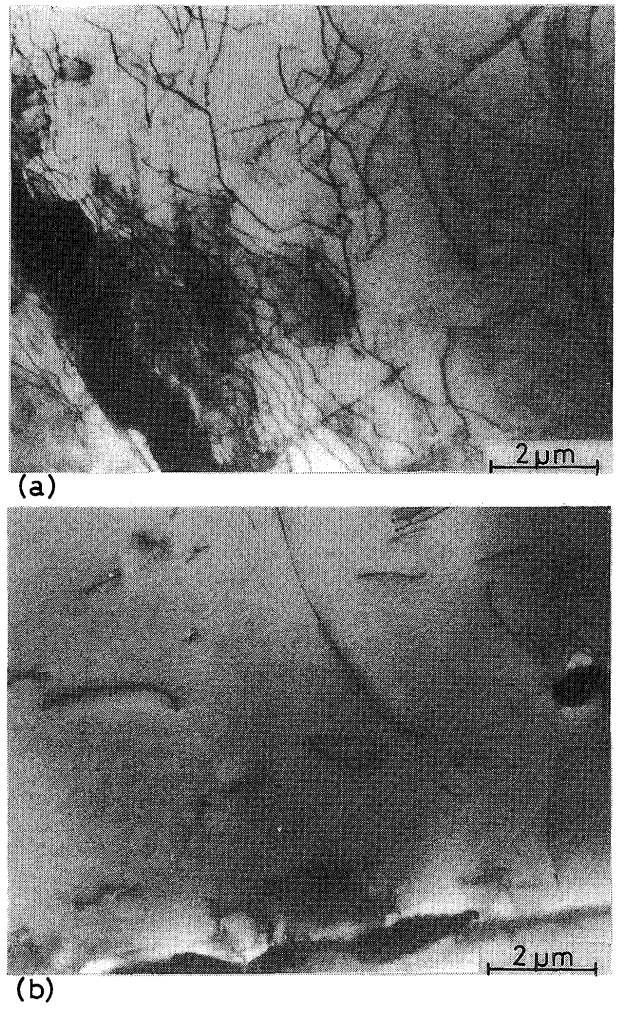

Fig.9 Electron microstructures in the steady state creep region ($\varepsilon \simeq 0.03$), (a) T = 1113K, σ_a = 44.1MPa, (b) T = 1213K, σ_a = 44.1MPa

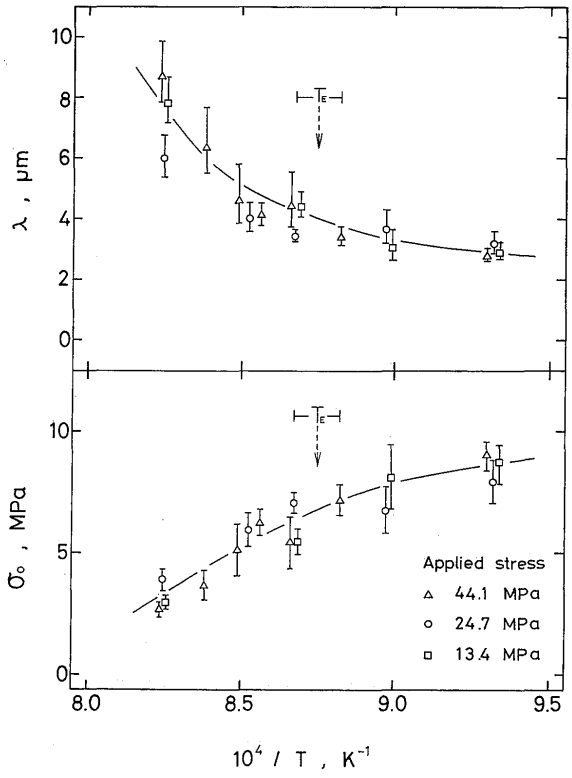

Fig.10 The variation of λ and σ_o calculated from eq. (14), with test temperature

3.6 Internal Back Stress, σ_i

Unfortunately, σ_i could not exactly be estimated, especially in the lower temperature range ($T < T_E$), because there were the large difference between σ_p and σ_n. The temperature dependence of σ_p and σ_n at σ_a = 34.7 MPa is shown in Fig.11. At temperatures lower than T_E, it appears that σ_i is close to σ_a and that the diffusion controlled dislocation creep mechanism is dominant. This is supported by the temperature dependence of $\dot{\varepsilon}_s$(Fig.3).

As seen in Fig.12, at $T > T_E$ and $\sigma_a \geqq 24.7$ MPa, σ_i is smaller than σ_a, but larger than σ_o, which has been estimated in Fig.10. $\sigma_i > \sigma_o$, even if σ_o is calculated by $\overline{M}$ = 3, and so σ_i cannot be explained by σ_o. If the average values of σ_p and σ_n are substituted for the internal stress σ_i under the conditions of [$T > T_E$ and $\sigma_a \geqq 24.7$ MPa], then $\sigma_e (= \sigma_a - \sigma_i)$, is larger than σ_o calculated by $\overline{M}$ = 3, in eq. (13). The mobile dislocations under the test condition of $T > T_E$ and $\sigma_a \geqq 24.7$MPa are not entirely stopped by the matrix particles. Therefore, the mobile dislocations are capable of overcoming (or bowing out from) them by the thermally activated motion. The mean slipping velocity of the mobile dislocations is reduced by the thermally activation motion. Probably, the mean velocity is related with the time, t_{wi}, necessary to pass along each particle. The reduction of the mean

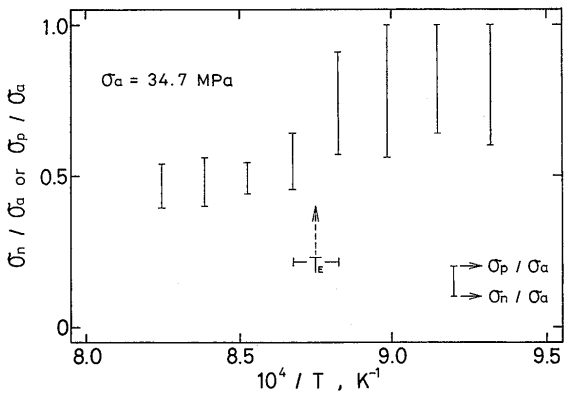

Fig.11 Temperature dependence of σ_p / σ_a and σ_n / σ_a at σ_a 34.7MPa

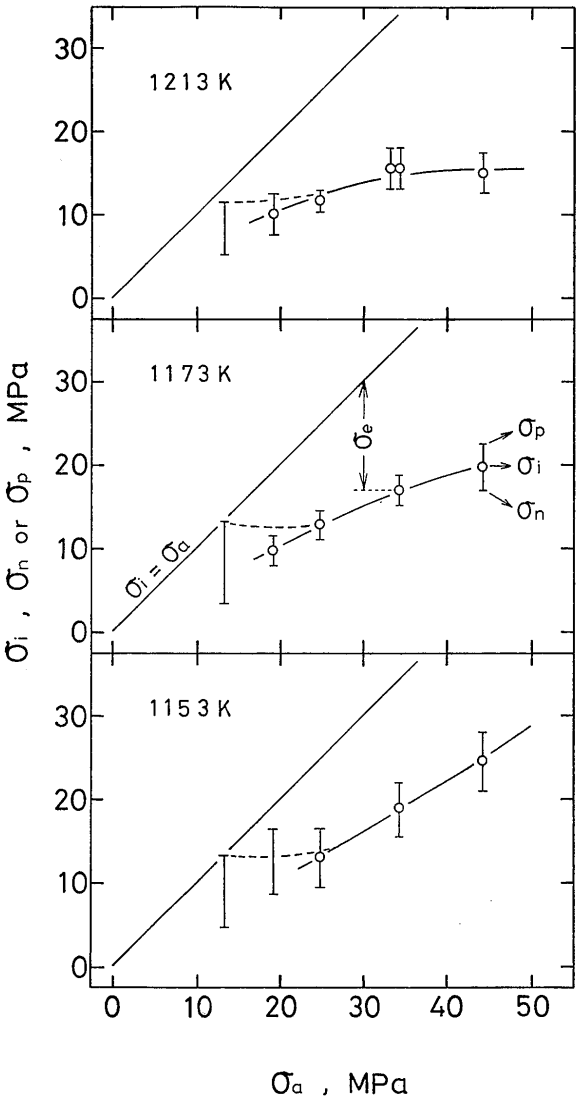

Fig.12 The variation of σ_p, σ_n, and σ_i with the applied stress

velocity causes the glide process of the mobile dislocations to be the rate-controlling step for the creep deformation at $T > T_E$ and $\sigma_a \geqq 24.7$MPa.

3.7 Steady State Creep Rate Rearrenged by Effective Stress and True Activation Energy for Creep

At temperatures above T_E, the effective stress, σ_e, inceases with increasing σ_a as indicated in Fig.12. The electron micrographs for $T > T_E$ suggest that the dislocation-structures in this condition do not consist of the dislocation-networks. So our experimental results for $T > T_E$ cannot be explained by the theory of Morris, who proposed the creep equation taking account of the change in dislocation structures[12].

The steady state creep rates for $T > T_E$, $\sigma_a \geqq 19.1$MPa are rearranged in Fig.13, by eq. (2). The experimental points for σ_a = 19.1MPa, however, deviate from the slope of $n_e (\simeq 4)$ determined from the results of $\sigma_a \geqq 24.7$MPa. This suggests that, in $T > T_E$, the creep deformation

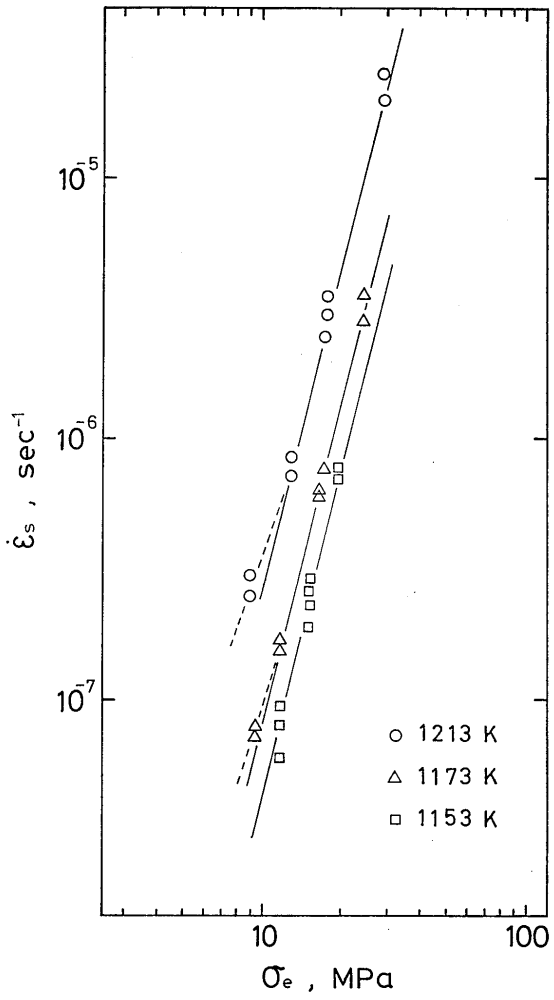

Fig.13 Dependence of the steady state creep rate , $\dot{\varepsilon}_s$, on the effective stress, σ_e

mechanism under the lower stress level ($\sigma_a < 19.1$MPa) is different from that of the higher stress level (24.7MPa $\leqq \sigma_a \leqq$ 44.1MPa).

For $\sigma_a \geqq 24.7$MPa and $T > T_E$, the true activation energy, Q_c^*, obtained from eq. (15) is 345kJ / mol, being larger than ΔH_{SD} of Fe. If the glide of the mobile dislocation is the rate-controlling step for the creep, this activation energy, Q_c^*, is not necessary to equal ΔH_{SD}.

4. Discussion

4.1 Creep Deformation for $T < T_E$ or $\sigma_a < 19.1$MPa

In $T < T_E$, plate-like precipitates cover grain boundaries, preventing mobile dislocations from sinking easily into them. The dislocations result in tangling or piling up at the locations adjacent to the grain boundaries. In this case, the creep cannot proceed, unless the internal back stress is reduced to the level of the applied stress by diffusion controlled recovery. The maximum of the internal stress is, therefore, equal to the applied stress in the steady state creep range. This consideration will be able to hold for the low stress level at $T > T_E$, because dislocations under the low stress level are not competent for sinking by themselves into grain boundaries which contain the dotted-precipitates.

The force-distance curve for $T < T_E$ or $\sigma_a < 19.1$MPa can be described, as like as Fig.14 (a). The stress field is periodically variable,[27,28] but the maximum is adjacent to the grain boundary. $\Delta\sigma_n$ at $T < T_E$ or $\sigma_a < 19.1$MPa is, idealistically, represented by Fig.14 (a). Matrix particles are only capable of reducing the mean velocity of mobile dislocations, and represented by vertical lines in Fig.14.

Now, let us consider processes 1 and 2 in Fig.15. Process 1 is the slip of intergranular dislocations. Process 2 is the climb of a dislocation with the help of diffusion. This diffusion is considered to be the lattice diffusion rather than the grain boundary diffusion, because the grain boundaries have been covered with the precipitates. In the lower stress level or at $T < T_E$, it is thought that process 2 is the rate-controlling process.

It is considered in the lower stress level that

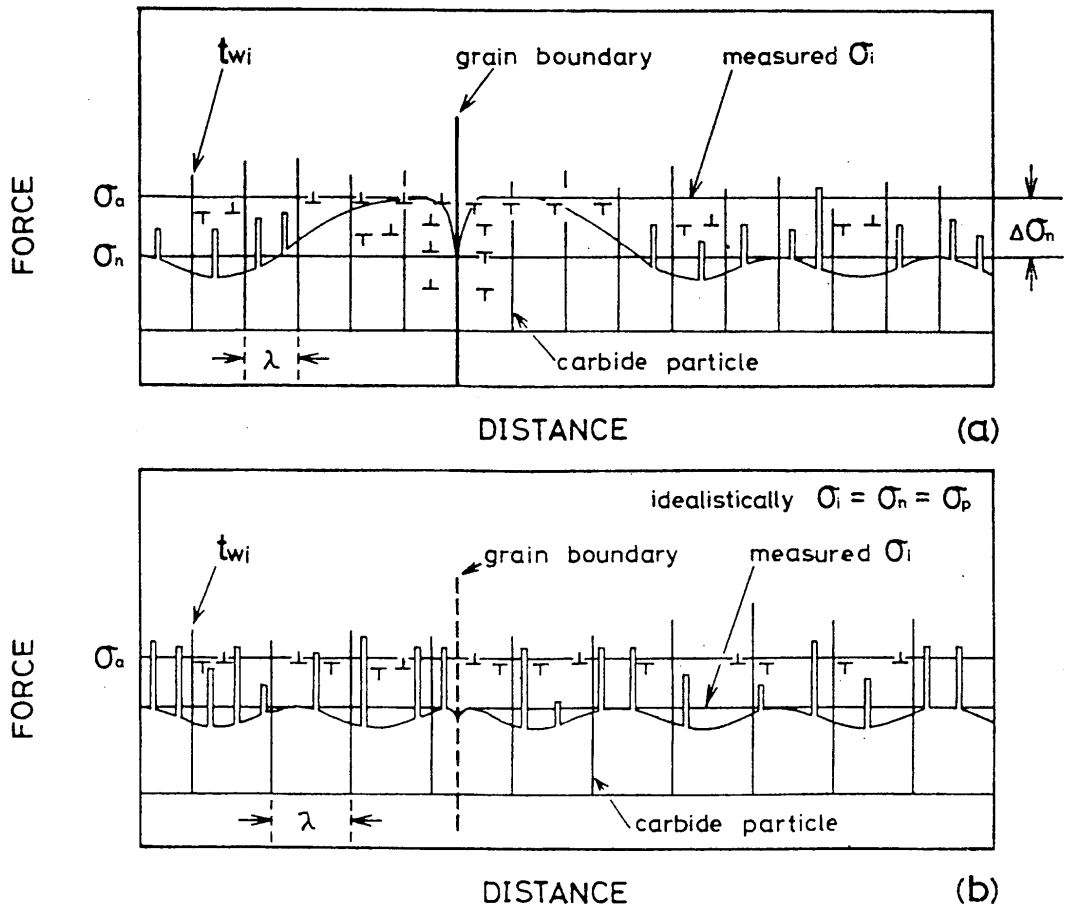

Fig.14 Schematic force-distance curve, (a) for $T < T_E$, or $T > T_E$ and $\sigma_a < 19.1$MPa, (b) for $T > T_E$ and $\sigma_a > 19.1$MPa

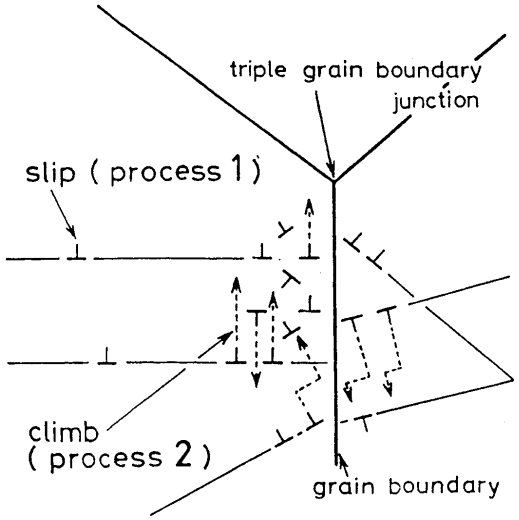

Fig.15 Schematic representation of creep deformation processes in $T<T_E$

dislocations climb at the location adjacent to grain boundaries, and annihilate one another or sink into grain boundaries, because the field of the tangles, where process 2 will occur, is narrow and near grain boundaries in the lower stress level. The climb-rate in this stress level will be described by[29-31]

$$V_C = Z \cdot \sigma_c \exp(-Q / RT) \quad (16)$$

where Z is a proper constant, σ_c the stress concentration ($\sigma_c \alpha \sigma_a^2 / \mu b$), and $Q = \Delta H_{SD}$. It is possible that Q is smaller than ΔH_{SD} when the grain boundary diffusion (the diffusion at the interface between matrix and boundary precipitate) influences the climb rate in some degree. The creep rate will be represented as follows;

$$\dot{\varepsilon}_s \alpha \sigma_a^2 \exp(-Q / RT) = \sigma_a^2 \exp(-\Delta H_{SD} / RT) \quad (17)$$

The similar equation can also be derived from Ivanov and Yanushkevich creep[32]. But the similar equation for a 3rd power creep, has been led by other climb theories[33,34]. In fact, the creep in the low stress condition may be more complex than expected. It is, however, suggested that the diffusional creep deformation, where the climb will be the rate-controlling process, is dominant. This suggestion will hold true even in the high stress level if T is less than T_E.

In the high stress condition ($\sigma_a \leqq 19.1$ MPa) at $T<T_E$, the area, where dislocations climb up, is expected to be broad, and so the creep rate is produced by so-called power low creep[32,33] and is described by

$$\dot{\varepsilon}_s = A \sigma_a^{4-5} \exp(-\Delta H_{SD} / RT) \quad (18)$$

4.2 Creep Deformation for $T>T_E$ and 19.1 MPa $< \sigma_a \leqq$ 44.1MPa

At temperatures above T_E, boundary precipitates are dotted on the grain boundaries after the creep tests.

If σ_a is sufficiently high, the dotted-precipitates do not prevent dislocations from sinking into grain boundaries, so much as the plate-like precipitates, Even if a pile-up occurs at the dotted-precipitates, the rate of process 2 is higher in some degree than that of process 1 since the temperature high enough ($T>1153$K). (It is of course that σ_a is so high that the diffusional recovery becomes the rate controlling process.)

The creep rate can be represented in terms of the effective stress rather than the applied stress, and the force-distance curve will be similar to Fig.5 of Ref.16 or Fig.1 of Ref.34, being shown in Fig.14 (b) for the present study. The time, t_{wi}, required for mobile dislocations to overcome or bow out around each particles by the thermally activated motion[35] is expressed by

$$t_{wi} = t_o \exp(\Delta H_i / RT) \quad (19)$$

where t_o is a constant, and ΔH_i the activation energy for the ith particle barrier. The sum, t_A, of the time necessary for mobile dislocations to slip thermally until they hit the next particle is given by

$$t_A = t_s \exp(\Delta G / RT) \quad (20)$$

where t_s is a constant, and ΔG the activation energy of the thermal glide of dislocations(ΔH_i and ΔG are assumed not to be overlapped, independent of σ_a, when the range of σ_a is not so wide.) . If $\overline{\Delta H}$ is defined as $\sum_i t_{wi} = A_o \exp(\overline{\Delta H} / RT)$, and also $B_o \exp(Q_c^* / RT)i = A_o \exp(\overline{\Delta H} / RT) + t_A$, then the mean velocity of the mobile dislocations will be represented as follows;

$$\bar{v} \alpha 1 / (t_A + \sum_i t_{wi}) = (1 / B_o) \exp(-Q_c^* / RT) \quad (21)$$

where A_o and B_o are a proper constant.

A general creep equation can be written by $\dot{\varepsilon}_s = \gamma \rho b \cdot \bar{v}$, where γ is a proper constant, ρ the density of the mobile dislocations, and b the Burger's vector[23]. The stress dependency of $\dot{\varepsilon}_s$ is also phenomenologically described as $\dot{\varepsilon}_s \alpha \sigma_c^{ne}$. Eq. (2) can be , therefore, admitted to be valid. In fact, eq. (2) can hold true for the results at $T>T_E$ and 24.7MPa $\leqq \sigma_a \leqq$ 44.1MPa. However, represents the activation energy Q_c^* in eq. (2), consists of $\overline{\Delta H}$ and ΔG. It is, therefore, higher than that for self-diffusion of Fe.

5. Conclusion

1. At temperatures below T_E ($T_E \sim 1143K$), the apparent activation energy for the creep is approximately equal to the activation energy for lattice diffusion of Fe in the stainless steel.
2. At temperatures above T_E, the apparent activation energy for the creep increases as the applied stress increases. This indicates that the creep deformation mechanism at the high stress level is different to the diffusional recovery creep under the low stress level.
3. The dominant creep mechanism changes at temperatures adjacent to T_E. In $T < T_E$, the diffusional recovery creep is dominant. On the other hand, in $T > T_E$ and $\sigma_a \geqq 24.7MPa$, the dislocation glide is the rate-controlling process.
4. It is indicated that Q_c^* called the true activation energy for creep in eq.(2) is not necessary to equal the activation energy for self-diffusion of Fe.

References

1) C. L. Clark and J. W. Freeman, Trans. Amer. Soc. Met., 1947, 38, 148.
2) F. Garofalo, R. W. Whitemore, W. F. Domis and F. von Gemmingen, Trans. AIME, 1961, 221, 310.
3) F. Garofalo, Trans. AIME, 1963, 227, 351.
4) Y. Imai and Y. Fujimura, J. Jap. Inst. Met., 1965, 29, 23.
5) G. J. Guarnieri, J. Miller and F. J. Vawter, Trans. Amer. Soc. Met., 1950, 42, 981.
6) K. R. Williams and I. R. Mclauchlin, J. Mater. Sci., 1970, 5, 1063.
7) J. M. Adamson and J. W. Martin, Met. Sci. J., 1974, 8, 332.
8) B. Russell, R. K. Ham, J. M. Silcock and G. Willoughby, Met. Sci. J., 1968, 2, 201.
9) I. R. Mclauchlin, Met. Sci. J., 1974, 8, 247.
10) O. K. Chopra and K. Natesan, Met. Trans., 1977, 8A, 633.
11) H. J. Kestenbach, W. Krause and T. L. da Silveira, Acta Met., 1978, 26, 661.
12) D. G. Morris, Acta Met., 1978, 26, 1143.
13) Y. Takahashi and T. Yamane, J. Mater. Sci., 1979, 14, 2818.
14) J. E. Dorn, J. Mech. Phys. Solids, 1954, 3, 85.
15) A. F. Smith and G. B. Gibbs, Met. Sci. J., 1968, 2, (2), 47.
16) J. P. Poirier, Acta Met., 1977, 25, 913.
17) M. Pahutovà, J. Čadek and P. Ryš , Scripta Met., 1977, 11, 1061.
18) R. L. Fullman, Trans. Met. Soc. AIME, 1953, 197, 447.
19) R. S. Gates and C. A. P. Horton, Mater. Sci. Eng., 1977, 27, 105.
20) Y. Imai and K. Masumoto, Bulletin of Jap. Institute Met., 1966, 5, (2), 121.
21) U. F. Kocks, Physics of Strength and Plasticity (edited by A. S. Argon), M. I. T. Press, Cambridge, 1969, p.143.
22) U. F. Kocks, Met. Trans., 1970, 1, 1121.
23) L. J. Cuddy and J. C. Raley, Acta Met., 1973, 21, 427.
24) S. K. Mitra and D. Mclean, Proc. R. Soc. in London, 1966, 295, (A), 288.
25) S. K. Mitra and D. Mclean, Met. Sci. J., 1967, 1, 192.
26) R. C. Gifkins, J. Mater. Sci., 1970, 5, 156.
27) H. Conrad, J. Metals, 1964, 16, 582.
28) H. Conrad, Mater. Sci. Eng., 1970, 6, 265.
29) A. K. Mukherjse, Mater. Sci. Eng., 1971, 8, 83.
30) J. Friedel, Dislocations, 1956, Gauthier-Villars, p.177.
31) R. C. Gifkins, Met. Trans., 1976, 7A, 1225.
32) J. Weertman, Rate Processes in Plastic Deformation of Materials (edited by J. C. M. Li and A. K. Mukherjee), 1975, p.315, No.4 in American Society for Metals.
33) J. Weertman, Trans. ASM, 1968, 61, 681.
34) U. F. Kocks, Rate Processes in Plastic Deformation of Materials, 1975, p.356, No.4 in Amer.Soc.Met.
35) R. J. Arsenault and T. Cadman, ibid, p.102.